

# A novel transient turbulent jet flame for studying turbulent combustion

Haifeng Wang<sup>a,\*</sup>, Mrinal Juddoo<sup>b</sup>, Sten H. Starner<sup>b</sup>,  
Assaad R. Masri<sup>b</sup>, Stephen B. Pope<sup>a</sup>

<sup>a</sup> Sibley School of Mechanical and Aerospace Engineering, Cornell University, Ithaca, NY 14853, USA

<sup>b</sup> School of Aerospace, Mechanical and Mechatronic Engineering, The University of Sydney, NSW 2006, Australia

Available online 29 August 2012

## Abstract

This paper introduces a new class of transient turbulent flames as a new benchmark case for studying turbulent combustion. It also brings together the latest high-speed laser imaging experiments with large-eddy simulation (LES)/probability density function (PDF) to advance the calculations of transient processes in the newly introduced test cases. The otherwise steady jet flames are subjected to a pulse of inflow velocity such that the flow experiences sequentially increased local extinction, the formation of upper and lower burning regions separated by a blown-off section, re-ignition and reconnection of the separated flame regions, and then the returning of the flame to statistical stationarity. The base test cases considered here are Sydney University's turbulent methane piloted flames L, B and M. The LES/PDF model predicts the flame's dynamic response to the velocity pulse qualitatively, with the extinction limit predicted accurately compared to the measurement. This paper reports the first LES/PDF calculations of these flames which have narrow reaction zones compared to Sandia's partially premixed flames, D, E and F. The statistically-transient jet flame introduced here provides a new benchmark for studying the effects of turbulence-chemistry interaction.

© 2012 The Combustion Institute. Published by Elsevier Inc. All rights reserved.

**Keywords:** Transient jet flames; High-speed imaging; Large-eddy simulation; Probability density function

## 1. Introduction

Turbulent combustion remains an important research subject due to its wide occurrence in

industrial applications such as ground transportation vehicles, aircraft engines, and power-generation plants. Considerable understanding of turbulent combustion has been gained in the past several decades via the advancement of laser diagnostics and high-performance computing technologies. Under the collaborative framework organized by the TNF workshop [1], a series of turbulent flames has been chosen as targets for the experimental and modeling studies, including the Sandia piloted flames D, E, and F [2], the Cabra lifted jet flame [3], and recently new targets have been identified such as the turbulent premixed stratified flame [4].

\* Corresponding author. School of Aeronautics and Astronautics, Purdue University, West Lafayette, IN 47906, USA. Fax: +1 607 255 1222.

E-mail addresses: [hw98@cornell.edu](mailto:hw98@cornell.edu) (H. Wang), [mrinal.juddoo@sydney.edu.au](mailto:mrinal.juddoo@sydney.edu.au) (M. Juddoo), [sten.starner@sydney.edu.au](mailto:sten.starner@sydney.edu.au) (S.H. Starner), [assaad.masri@sydney.edu.au](mailto:assaad.masri@sydney.edu.au) (A.R. Masri), [s.b.pope@cornell.edu](mailto:s.b.pope@cornell.edu) (S.B. Pope).

Collaborative research on these target flames has led to significant progress in the development and validation of turbulent combustion models.

Statistically-stationary flames have many advantages in that they do not depend on initial conditions and have good reproducibility. Measurements of different quantities can be made separately without synchronization and with single-shot techniques. Additionally, the statistics can be collected in time, and the direct quantitative comparison between the model predictions and measurement is straightforward. Stationary flames can be studied under different conditions with different Reynolds and Damköhler numbers, and can be used to validate a wide range of models with different applicability. Good examples are the Sydney piloted methane flames L, B, and M [5,6] and the Sandia piloted flame series D, E, and F [2]. In these series, flames L and D are burning healthily, flames B and E exhibit significant local extinction, and flames M and F have severe local extinction and are close to blow-off. Flames L and D are often used to validate turbulent combustion models applicable to high Damköhler number (e.g., the steady flamelet model [7]), while flames B and E, and M and F are very challenging and are used to validate models applicable also to moderate or low Damköhler number and with strong turbulence-chemistry interactions (e.g., the probability density function methods [8–10]).

It is noted that while statistically stationary flames will remain important targets for model development, they are limited in scope and do not account for transient phenomena which are observed in many applications. The start-up and shut-down processes of any combustor are not statistically stationary. During the acceleration or deceleration of an aircraft, the flow rates of fuel injection and air are adjusted to produce the desired thrust. In a reciprocating engine, the combustion process goes through a combustion cycle periodically that is strongly time dependent. Studying statistically transient turbulent combustion is, therefore, of significant practical interest and forms the subject matter of this paper. Certainly, transient flames relevant to reciprocating internal combustion (IC) engines have been studied extensively, e.g., turbulent flame balls [11,12]. It is noted that these transient flames relevant to IC engines are different from the transient flames introduced below as explained in the later discussion.

Large-eddy simulation and high-speed laser imaging [13–20] may now be brought together to study the new class of turbulent transient flames introduced here. It should be noted that large-eddy simulation (LES)/probability density function (PDF) methods [8–10,21] are inherently time-dependent and hence applicable to statistically-transient flames. However, these transient test cases present a challenge for the LES/PDF

method to compute the entire sequence of transitions from fully burnt to fully extinguished states at the correct times. For simplicity, the design of the transient flames is built upon the existing canonical flows with statistically time-dependent boundary conditions. This is different from traditional combustion in IC engines in that the flows studied here transition through a range of states from conditions of steady burning to a fully extinguished state and then back to steady burning. The ability to cover the entire range of flow conditions, including a smooth transition between fully-burnt and fully-extinguished states, is a novelty of this experiment.

Another key contribution of this paper is that it reports the first LES/PDF calculations of turbulent non-premixed flames of methane approaching blow-off, namely the Sydney University flame series. These are more challenging than Sandia's partially premixed flames series D, E and F due to the narrow reaction zones associated with pure methane fuel.

The paper is organized as follows: The pulsed piloted burner configuration is presented in Section 2, followed by the modeling of Sydney piloted flame L in Section 3 which is performed in order to establish a base case for the statistically-transient jet flame. The experimental and modeling studies of the new transient jet flame are presented in Section 4, and the conclusions are drawn in Section 5.

## 2. The pulsed piloted burner

The basic platform is the Sydney piloted burner which has been used extensively to stabilize flames at different departures from blow-off [5,6]. Typical examples are methane flames L, B, M and the well-known partially premixed methane-air flames D, E and F. A key feature of these series is that, with increasing jet velocity, local extinction leading to global blow-off occurs in a flame region downstream of the stabilizing pilot. The focus of this paper is on methane flames L, B, M which are challenging in their own right because of their narrow reaction zones and have never been computed before using the LES/PDF approach. Only a brief description of the burner is given here and full details may be found elsewhere [5,6].

The Sydney piloted flame burner has a central jet of fuel (diameter  $D = 7.2$  mm) supplied with pure  $\text{CH}_4$ . The jet is surrounded by a stoichiometric premixed and fully burnt annulus of  $\text{C}_2\text{H}_2$ ,  $\text{H}_2$ , and air with C/H ratio to that of methane hence resulting a higher enthalpy. This higher enthalpy in the pilot stream is not problematic for the current LES/PDF modeling but causes difficulty with flamelet modeling approaches [7]. The outer diameter of the annulus is 18 mm, and the bulk velocity of the unburnt pilot gas is 3 m/s,

from which the bulk velocity of the burnt pilot can be calculated to be about 22.8 m/s assuming equilibrium with 5% heat loss to the burner. A coflow of air with a speed of 15 m/s is maintained outside the burner. The use of a fixed pilot velocity (3 m/s unburnt) and a higher co-flow velocity are two features of difference between flames L, B, M and flames D, E, F. Detailed measurements of the flow and scalar fields in flame L are reported in [5,6] and a comprehensive experimental data set [5,6,22] is available for model validation. It is worth noting here that this data set which was collected in the 1980s was based on Raman–Rayleigh scattering so the uncertainty in CO and H<sub>2</sub>, due to interferences, is higher than that in temperature and the remaining measured species.

Flame L with a bulk jet velocity of  $U_L = 41$  m/s is used here as a base case. A time-dependent additional inflow is then imposed on this base case so that the jet bulk velocity varies in time as  $U(t) = U_L(1 + f(t))$ , where  $f(t)$  is the shape of the imposed variation to the bulk velocity. The objective of this study is to describe the response of the flame to the inflow variation. A velocity pulse variation is applied, subject to which the flame experiences increased local extinction, blow-off, and re-ignition. The particular form of  $f(t)$  used here is shown in Fig. 1 and the timing details are described later in Section 4. The increase in  $f(t)$  leads to flame blow-off, then, as  $f(t)$  decreases, the flame re-ignites, and eventually returns to flame L. The velocity pulse is chosen for the experimental convenience. Other shapes can be applied but may have some technical difficulties to implement experimentally. With modeling studies, there is no restriction to the variation of the pulse shape, and this can also be applied to other parameters such as temperature and composition in the different inflow streams. Furthermore, the idea can be applied to different existing flames with different configurations such as turbulent premixed flames

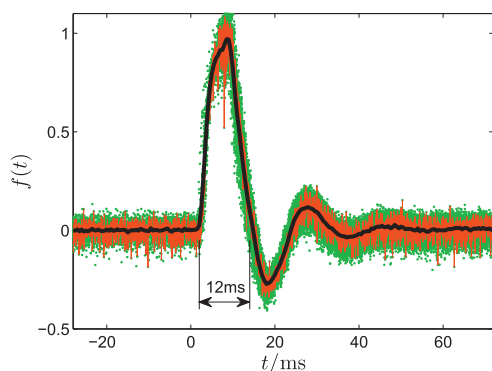


Fig. 1. The temporal variation function  $f(t)$  (thick solid line) obtained from averaging 20 measurements (dots). An individual realization is also shown as the thin solid line which fits within the scatter of the dots.

[23], turbulent lifted jet flames [3], and turbulent opposed jet flames [24]. In this work, we study only the Sydney piloted flame subject to the jet velocity pulse to demonstrate the new approach.

This new class of transient jet flames offers a compact method for studying combustion and its interaction with turbulence. Subject to a proper inflow velocity variation, these flames allow transition from extinction to re-ignition in a well controlled configuration so they cover the entire range of statistically-stationary flames studied earlier, such as Sandia D, E, and F [2] and the Sydney L, B, and M [5,6] flames. They are more challenging test cases than stationary ones, and require a time-accurate representation of the combustion process, which has not been comprehensively validated for turbulent combustion modeling in past studies.

### 3. Modeling of Sydney piloted flame L

The modeling strategy consists of large-eddy simulations (LES) [8,25] and probability density function methods (PDF) [8–10]. LES defines a cut-off scale to separate large scales of turbulent motions and small ones with the former being explicitly resolved and the latter modeled. Since the large turbulent eddies contain most of the turbulent kinetic energy, LES is able to capture large-scale flow features which are of most practical interest. By introducing spatial filtering, a set of LES equations that governs the large-scale motions can be derived from the Navier–Stokes equation. The effect of sub-filter stresses is modeled by the dynamic Smagorinsky model (see [8]). Combustion occurs at very small scales that are not resolved in LES and hence requires modeling which imposes a great challenge to LES for turbulent combustion modeling. The PDF method [8–10] is one of the attractive combustion sub-models for LES. The joint conditional PDF of compositions  $\Phi = (\phi_1, \phi_2, \dots, \phi_n)$  for  $n$  components is defined as  $f(\Psi|\tilde{\mathbf{u}}; \mathbf{x}, t)$  with  $\Psi$  being the sample phase variable corresponding to  $\Phi$  and the conditioning variable  $\tilde{\mathbf{u}}$  the filtered velocity, and the transport equation for  $f(\Psi|\tilde{\mathbf{u}}; \mathbf{x}, t)$  is derived and modeled [10]. The effect of chemical reaction is treated exactly in the PDF method while the effect of the unclosed conditional molecular-diffusion term is modeled by mixing models.

The governing equations resulting from the above LES/PDF method are in closed form, and can be integrated in time to simulate turbulent reactive flows. For solving the LES equations, we adopt second-order central finite-difference schemes for the discretization. The Crank–Nicolson scheme is used for the time-advancement. More details of the LES solutions can be found in [21,25]. The Lagrangian Monte Carlo particle method [9] is usually used to solve the PDF equa-

tion. The stochastic particles evolve in physical space and in composition space, and the joint PDF is represented by the particle distributions. From the particle ensemble averages, different statistics can be formed. The particle method is implemented in a recently developed parallel Monte Carlo PDF particle solver called HPDF [21]. The simulations are performed in a cylindrical coordinate system with the computational domain being a cylinder of size  $[0, 60D] \times [0, 20D] \times [0, 2\pi]$  in the axial, radial and azimuthal directions. The domain is divided into  $144 \times 108 \times 48$  structured grid cells in the corresponding three directions with grid clustering in the flame zone and high gradient regions. The turbulent jet inflow condition is generated from a separate simulation of a fully-developed turbulent pipe flow with the same Reynolds number as the central jet flow. Thirty particles per cell are used in the HPDF solver, resulting in about 22 million particles in total. The selection of the above grid and the number of particles per cell is justified below. The molecular transport properties (kinematic viscosity  $\nu$  and molecular diffusivity  $\Gamma$ ) are obtained from an empirical fit to mean temperature [21]. The sub-filter diffusivity  $\Gamma_t$  is calculated from  $\Gamma_t = \nu_t / Sc$  where  $\nu_t$  is the sub-filter viscosity obtained from the dynamic Smagorinsky model and  $Sc = 0.4$  is the Schmidt number. The molecular transport is implemented using the random-walk model [26] with the effective diffusivity  $\Gamma_e = \Gamma + \Gamma_t$ . The detailed finite-rate chemistry is described by GRI-Mech 1.2 [27] and the mixing term is modeled by the modified Curl mixing model [28,29] with the mixing frequency  $\Omega$  modeled as  $\Omega = C\Gamma_e/2\Delta^2$  [21] where  $C = 4$  and  $\Delta$  is the filter width. The ISAT algorithm [30] is used to accelerate the chemistry calculations. The full-scale LES/HPDF simulations are performed on a parallel computing system with message-passing handled via MPI. The overall computational cost for simulating flame L is about a week on 864 cores ( $\sim 150,000$  CPU hours).

A sensitivity study is performed here for the effect of the grid resolution and the number of particles per cell  $N_{pc}$ . For the grid resolution study, we use LES with the flamelet model with the presumed PDF method [7] for computational efficiency. The results for three grid sizes are shown in Fig. 2 (left column). The base grid  $144 \times 108 \times 48$  produces slightly different results from those with the finer grids but the relative difference is smaller than 10%. For the purpose of this study, the base grid is taken as an appropriate choice with reasonable computational requirement. For the effect of  $N_{pc}$ , we use LES/PDF with the flamelet model to represent the thermochemical states [21]. Three values of  $N_{pc}$  (=30, 40, and 60) are tested and the results are shown in Fig. 2 (right column). It is evident that the results are not sensitive to the tested values of  $N_{pc}$ , and the

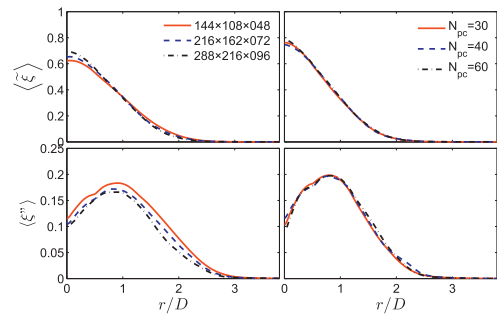


Fig. 2. Radial profiles of the mean and rms mixture fraction  $\langle \xi \rangle$  and  $\langle \xi'' \rangle$  at  $x/D = 20$ , with the different grids and with  $N_{pc} = 30$  (left column) and with the different number of particles per cell  $N_{pc}$  and with the grid  $144 \times 108 \times 048$  (right column).

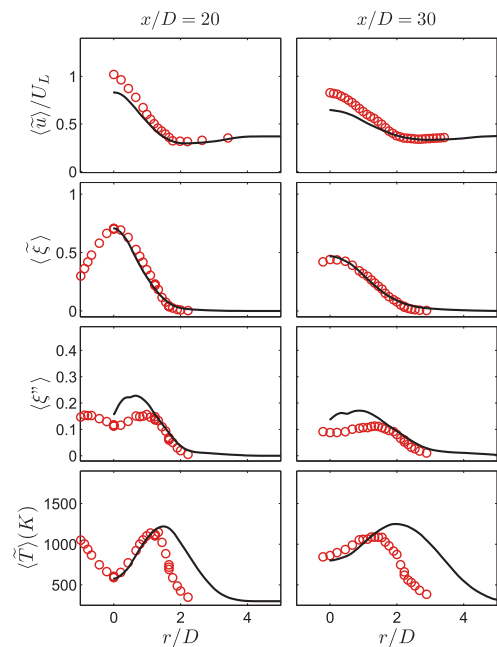


Fig. 3. Radial profiles of the time-averaged resolved axial velocity  $\langle \bar{u} \rangle / U_L$ , mixture fraction  $\langle \xi \rangle$ , total rms mixture fraction  $\langle \xi'' \rangle$ , and temperature  $\langle T \rangle$  at the axial locations of  $x/D = 20$  and 30 in flame L. Symbols: experimental data [5,6,22]; Lines: current LES/PDF results.

relative differences computed with  $N_{pc} = 30$  and 60 are within 3%. The choice of 30 particles per cell for the later studies is therefore justified.

Previous numerical simulation studies of flame L were reported in [31–33] with the PDF methods in the context of Reynolds averaged Navier–Stokes (RANS). Koutmos [34] reported simulations of flame L with a “2D” LES com-

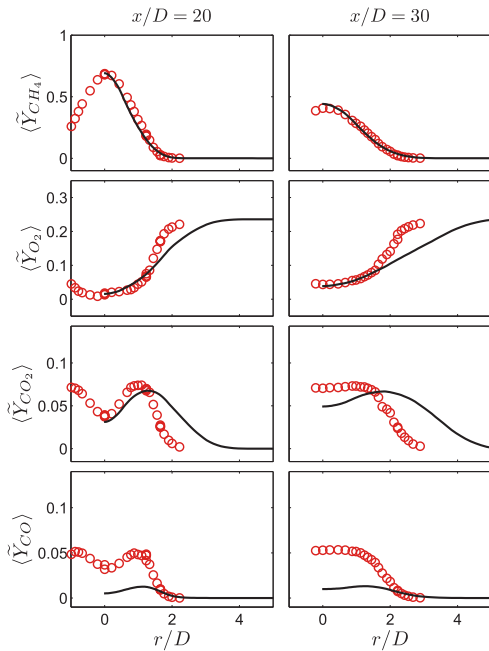


Fig. 4. Radial profiles of the time-averaged resolved mass fractions of CH<sub>4</sub>, O<sub>2</sub>, CO<sub>2</sub>, and CO at the axial locations of  $x/D = 20$  and  $30$  in flame L. Symbols: experimental data [5,6,22]; Lines: current LES/PDF results.

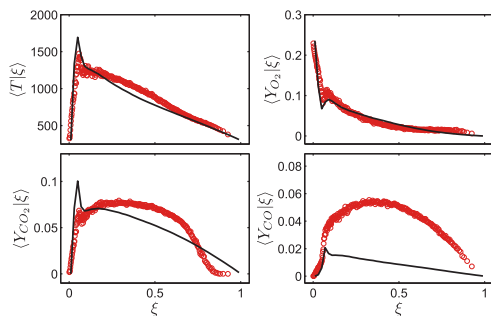


Fig. 5. Conditional means of temperature and species mass fractions of O<sub>2</sub>, CO<sub>2</sub>, and CO at the axial location of  $x/D = 20$  in flame L. Symbols: experimental data [5,6,22]; Lines: current LES/PDF results.

bin with a presumed PDF method. No LES/PDF studies of this flame have been reported in the literature and we present here the first set of LES/PDF/ISAT simulations of flame L.

Figure 3 shows the radial profiles of the time-averaged resolved axial velocity  $\langle \tilde{u} \rangle / U_L$ , mixture fraction  $\langle \tilde{\xi} \rangle$ , total rms mixture fraction  $\langle \tilde{\xi}'' \rangle$ , and temperature  $\langle \tilde{T} \rangle$  at the axial locations of  $x/D = 20$  and  $30$  in flame L where the most interesting flame dynamics occur. The axial velocity is under-predicted by the current modeling

method, especially near the axis. The mixture fraction is accurately predicted with the rms mixture fraction  $\langle \tilde{\xi}'' \rangle$  slightly over-predicted. The temperature prediction is reasonable with the predicted peak values shifted outward compared to the experimental data. The predictions of species mean mass fractions of CH<sub>4</sub>, O<sub>2</sub>, CO<sub>2</sub>, and CO are compared in Fig. 4. With the exception of CO which is discussed below, the discrepancy between the model predictions and the experimental data is consistent with the predictions of flow, mixing and temperature fields in Fig. 3.

The turbulence-chemistry interactions that are crucial to turbulent combustion modeling can be better represented in mixture fraction space as shown in Fig. 5. The agreement between the measurement and LES/PDF predictions is apparently much improved in mixture fraction space although there is still evident discrepancy in the fuel-rich side, especially for CO. Possible causes of this discrepancy could be (i) the effect of differential-diffusion that is not accounted for in this study, (ii) uncertainty in the imposed pilot inflow boundary conditions, and (iii) uncertainties in the CO measurements. A detailed parametric LES/PDF study will be performed in the future to analyze and understand the reasons underlying these observed discrepancies. It is worth noting however, that the overall discrepancy noted in this study is consistent with that reported earlier for calculations that use the RANS/PDF method [31–33]. For flame L, the overall flow, mixing and reacting fields are reasonably represented by the current LES/PDF method, and are sufficiently good to demonstrate the studies of the transient case in the next section.

#### 4. Turbulent transient jet flame

The turbulent transient jet flame is based on the previous statistically-stationary jet flame L. Experimentally, a rapid pulse of additional fuel is imposed on the base flow for condition L at some distance upstream of the jet exit plane. With all other conditions kept unchanged, this results in a bulk velocity profile at the jet exit plane of the form  $U(t) = U_L(1 + f(t))$ . The variation function  $f(t)$  used here is shown in Fig. 1 and this is obtained from averaging over 20 repetitions of the experimental measurements of the centerline jet exit velocity obtained using laser Doppler velocimetry (LDV). The duration of the main pulse is about 12 ms, and it takes about 40 ms to dampen the subsequent oscillations and return to the statistically-stationary state. The good reproducibility of the pulse is confirmed by the repeated measurements as shown in Fig. 1, in which an individual realization is shown as the thin solid line, and all the samples from the 20 measurements are shown as dots. Two typical

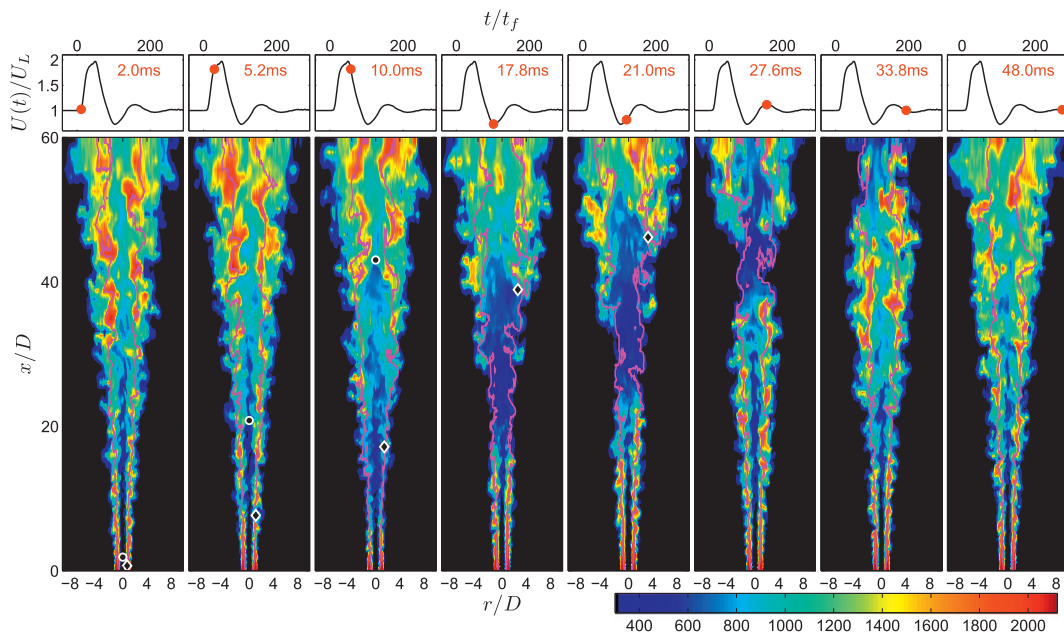


Fig. 6. Snapshots of temperature from the LES/PDF simulation of the transient jet flame at different times that are indicated by the symbols on the top-row subplots. The solid lines on the plot are the iso-line of the stoichiometric mixture fraction 0.055. Two fluid markers denoted by the symbols ( $\circ$  and  $\diamond$ ) are released at  $t = 0$  at the jet exit plane  $x/D = 0$ , and follow the velocity at the centerline and the velocity on the iso-line of stoichiometric mixture fraction, respectively. (An animation of the images is included in the Supplemental data of this paper.)

time scales associated with the transient case are, the flow time scale  $\tau_f = D/U_L \approx 0.18$  ms, and the time scale of the pulse  $\tau_p = 12$  ms which is much larger than the flow time scale  $\tau_f$ .

The LES/PDF simulations are performed for the transient jet flame subject to the pulse in Fig. 1. The jet inflow boundary condition that is obtained from a fully developed pipe flow simulation is multiplied by  $1 + f(t)$ . The initial condition is set to be the statistically-stationary solution of flame L obtained in the previous section, and the simulation starts at  $t = 0$  in Fig. 1 and ends at about  $t = 60$  ms to cover the transition.

For the model comparison, high-speed (5 kHz) OH images of planar laser-induced fluorescence (OH-PLIF) are taken during the flame transition subject to the pulse. Excitation of OH was achieved using the  $Q_1(6)$  line of the  $A^2\Sigma \leftarrow \chi^2\Pi(1,0)$  system. The desired wavelength was obtained by using a high-speed Edge-wave (IS4II-E) Nd:YAG laser, with an average power of 12 W, to pump a dye laser running with Rhodamine 6G in ethanol. The fundamental output of the dye laser at 566 nm was then frequency doubled to produce a UV beam at 283.01 nm, with an average power of 750 mW at 5 kHz (150  $\mu$ J/pulse). Full details about the high-speed OH-PLIF imaging system are given elsewhere [19].

Figure 6 shows snapshots of temperature from the LES/PDF simulation of the transient jet flame

subjected to the pulse in Fig. 1, with the timing indicated on the top row of Fig. 6. The contour of the stoichiometric mixture fraction of 0.055 is also shown in the figure. Two markers denoted by the symbols (circle and diamond) are also shown in the figure to follow, respectively, the instantaneous velocity at the centerline and at the stoichiometric mixture fraction. These markers show the distance from the jet exit plane travelled by the fluid at these respective locations. An animation corresponding to Fig. 6 is included in the Supplemental data of this paper. For the statistically-stationary flame, the jet bulk velocity that leads to global extinction in the experiment is about 68 m/s. In the current transient case, the bulk jet velocity increases to about 80 m/s which is well above the steady blow-off limit. From Fig. 6, we can observe the flame's evolution subject to the pulse. Initially, the flame is in a statistically-stationary state exhibiting some local extinction that can be seen from the disconnected high-temperature regions along the stoichiometric mixture fraction contour. With the increase of the inflow bulk velocity  $U(t)$ , the amount of local extinction increases, e.g., at  $t = 10.0$  ms when  $U(t)$  just starts to decrease, severe local extinction is observed between  $x/D \in (10, 20)$ . A fully extinguished band that extends for about 10 jet diameters from just downstream of the pilot at  $t = 10.0$  ms and moves downstream such that

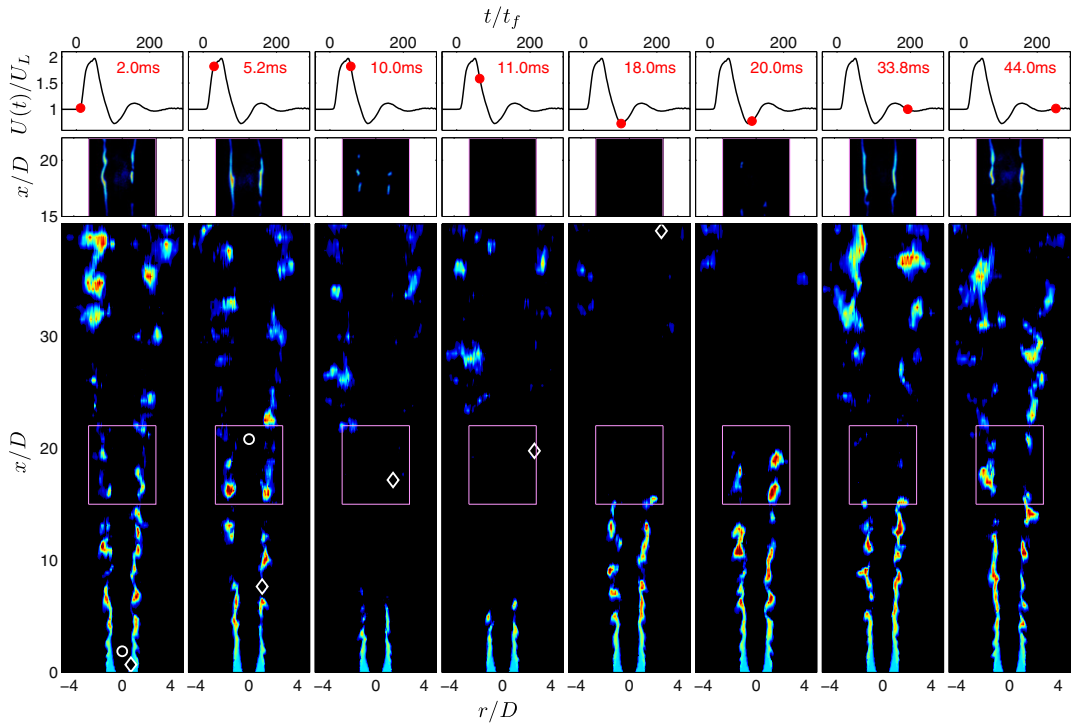


Fig. 7. Snapshots of OH from the experiment (middle row) and from the LES/PDF simulation (bottom row) of the transient jet flame at different times that are indicated by the symbols on the top-row subplots. Two fluid markers denoted by the symbols ( $\circ$  and  $\diamond$ ) are released at  $t=0$  at the jet exit plane  $x/D=0$ , and follow the velocity at the centerline and the velocity on the iso-line of stoichiometric mixture fraction, respectively. (An animation of the images is included in the Supplemental data of this paper.)

at  $t=21.0$  ms this band extends from about  $x/D=20$  to 30. It is worth noting that, at this time, the pulse has already moved beyond the first minimum. The flame is now clearly separated into an upstream and downstream burning regions. At  $t=27.6$  ms, the pulse reaches a minor peak and the flame starts to reconnect via the re-ignition of the upstream region now that the velocity has decreased. The mechanism of re-ignition depends on the local condition of the mixture that exists in the region downstream of the pilot at the times when the strain rates are relaxed. When fully analyzed, the wealth of information available in the simulations will provide an explanation of the dominant re-ignition mechanism.

High-speed OH-PLIF imaging is performed experimentally to assess the current LES/PDF simulations. The snapshots of OH in the transient jet flame are compared in Fig. 7 with a corresponding animation shown in the Supplemental data. The OH-PLIF imaging is obtained within a rectangular region of  $x/D \in (15, 22)$  and  $r/D \in (-2.78, 2.78)$ , and the sequences of OH images are shown in the middle row of Fig. 7. The bottom row shows the LES/PDF results with the region for the measurement marked within as a rectangle. The images from the experiment and

simulation are synchronized and the timing is shown on the top row of Fig. 7. The direct comparison between the OH measurement and simulation is only qualitative since the current OH-PLIF is not quantified. However, quantitative comparison can be made for the timing of the extinction and ignition events. From the experiment in the middle row of Fig. 7 and the animation in the Supplemental data, we can see that extinction occurs at about  $t=10.2$  ms inside the measured region and re-ignition starts to occur at about  $t=20.0$  ms. This gives a duration of extinction for about 10 ms, which is roughly the same as the duration of the pulse  $t_p=12$  ms. In the LES/PDF simulations, extinction starts to occur (inside the measured region) at about  $t=10.0$  ms, coinciding with the measured extinction limit. Re-ignition occurs at about  $t=18.0$  ms which is 2 ms earlier than observed experimentally. This is a minor difference which is, nevertheless, an indication of early ignition in the LES calculations. At the later time of  $t=33.8$  ms, the LES shows a second extinction event in the calculations possibly due to the second peak of the pulse, which is not observed in the experiment. This trend of easy extinction is consistent with previous PDF simulations [35]

using the same mixing model. Similarly, the early ignition is consistent with previous PDF simulations of a lifted jet flame [36]. The performance of different mixing models on this much more challenging flame needs to be assessed, and improvement is likely needed to capture the re-ignition time accurately.

The first set of LES/PDF and LIF-OH results reported here highlight the interesting features of flame evolution and response to the imposed disturbances. It is evident from these results that this novel approach along with the coupling between LES and high-speed imaging diagnostics provides a powerful tool for studying statistically-transient turbulent combustion phenomena.

In future work, further model assessment and sensitivity analysis will be performed to improve model predictions. Studies will be conducted for both measurements and simulations based on multiple realizations to generate full statistical descriptions of the flame dynamics. Different types of pulses with different amplitudes and time-scales will also be considered to explore the effects of a broader range of disturbances.

## 5. Conclusions

A new class of transient jet flames is introduced for the study of turbulent combustion. A collaborative study with high-speed imaging measurements and LES/PDF simulations is performed for a turbulent non-premixed transient jet flame that is based on the Sydney piloted flame L. A pulse of jet inflow velocity is imposed on the otherwise stationary flow, and the response of the flame to the pulse is studied. Subject to the velocity pulse, the flame exhibits sequentially increased local extinction, upper and lower burning regions separated by a section where extinction occurs, re-ignition and reconnection of the separated flame regions, and returning to the statistically-stationary flow. The LES/PDF modeling approach qualitatively predicts the sequence of flame dynamics. The predicted extinction occurs at about the same time as the measurements albeit for a slightly shorter duration. The transient jet flame introduced here is demonstrated to be well-suited for the studies of combustion and its interaction with turbulence, and to provide a new class of more challenging benchmark flames for the future modeling studies.

## Acknowledgments

This research is supported by the Combustion Energy Frontier Research Center, an Energy Frontier Research Center funded by the U.S. Department of Energy, Office of Science, Office

of Basic Energy Sciences under Award No. DE-SC0001198. The work at Sydney was supported by the Australian Research Council. The research used resources of the Oak Ridge Leadership Computing Facility, located in the National Center for Computational Sciences at Oak Ridge National Laboratory, which is supported by the Office of Science of the Department of Energy under Contract DE-AC05-00OR22725.

## Appendix A. Supplementary data

Supplementary data associated with this article can be found, in the online version, at <http://dx.doi.org/10.1016/j.proci.2012.06.021>.

## References

- [1] International workshop on measurement and computation of turbulent nonpremixed flames, <http://www.sandia.gov/TNF/abstract.html>.
- [2] R.S. Barlow, J.H. Frank, *Proc. Combust. Inst.* 27 (1998) 1087–1095.
- [3] R. Cabra, T. Myhrvold, J.-Y. Chen, R.W. Dibble, A.N. Karpetsis, R.S. Barlow, *Proc. Combust. Inst.* 29 (2002) 1881–1888.
- [4] F. Seffrin, F. Fuest, D. Geyer, A. Dreizler, *Combust. Flame* 157 (2010) 384–396.
- [5] A.R. Masri, R.W. Bilger, R.W. Dibble, *Combust. Flame* 81 (1990) 260–276.
- [6] A.R. Masri, R.W. Dibble, R.S. Barlow, *Prog. Energy Combust. Sci.* 22 (1996) 307–362.
- [7] N. Peters, *Prog. Energy Combust. Sci.* 10 (1984) 319–339.
- [8] S.B. Pope, *Turbulent Flows*, Cambridge University Press, 2000.
- [9] S.B. Pope, *Prog. Energy Combust. Sci.* 11 (1985) 119–192.
- [10] S.B. Pope, *J. Fluid Mech.* 652 (2010) 139–169.
- [11] S.B. Pope, W.K. Cheng, *Proc. Combust. Inst.* 21 (1988) 1473–1481.
- [12] C.K. Law, G. Jomaas, J.K. Bechtold, *Proc. Combust. Inst.* 30 (2005) 159–167.
- [13] M.W. Renfro, G.B. King, N.M. Laurendeau, *Appl. Optics* 38 (1999) 4596–4608.
- [14] J. Hult, U. Meier, W. Meier, A. Harvey, C.F. Kaminski, *Proc. Combust. Inst.* 30 (2005) 701–709.
- [15] M. Tanahashi, S. Murakami, G.-M. Choi, Y. Fukuchi, T. Miyauchi, *Proc. Combust. Inst.* 30 (2005) 1665–1672.
- [16] C. Kittler, A. Dreizler, *Appl. Phys. B* 89 (2007) 163–166.
- [17] I. Boxx, C. Heeger, R. Gordon, et al., *Proc. Combust. Inst.* 32 (2009) 905–912.
- [18] B. Bohm, C. Heeger, I. Boxx, W. Meier, A. Dreizler, *Proc. Combust. Inst.* 32 (2009) 1647–1654.
- [19] M. Juddoo, A.R. Masri, *Combust. Flame* 158 (2011) 902–914.
- [20] N. Jiang, R.A. Patton, W.R. Lempert, J.A. Sutton, *Proc. Comb. Inst.* 33 (2011) 767–774.
- [21] H. Wang, S.B. Pope, *Proc. Combust. Inst.* 33 (2011) 1319–1330.

- [22] Sydney flame database, <http://sydney.edu.au/engineering/aeromech/thermofluids/database.htm>.
- [23] Y.-C. Chen, N. Peters, G.A. Schneemann, N. Wruck, U. Renz, M.S. Mansour, *Combust. Flame* 107 (1996) 223–244.
- [24] G. Coppola, B. Coriton, A. Gomez, *Combust. Flame* 156 (2009) 1834–1843.
- [25] C.D. Pierce, P. Moin, *J. Fluid Mech.* 504 (2004) 73–97.
- [26] M.S. Anand, S.B. Pope, *Turbul. Shear Flow* 4 (1985) 46–61.
- [27] M. Frenklach, H. Wang, C.-L. Yu, et al., [http://www.me.berkeley.edu/gri\\_mech](http://www.me.berkeley.edu/gri_mech).
- [28] J. Janicka, W. Kolbe, W. Kollmann, *J. Non-Equilib. Thermodyn.* 4 (1979) 47–66.
- [29] P.A. Nooren, H.A. Wouters, T.W.J. Peeters, D. Roekaerts, U. Maas, D. Schmidt, *Combust. Theory Model.* 1 (1997) 7996.
- [30] S.B. Pope, *Combust. Theory Model.* 1 (1997) 41–63.
- [31] A.R. Masri, S.B. Pope, *Combust. Flame* 81 (1990) 13–29.
- [32] W.P. Jones, M. Kakhi, *Combust. Flame* 115 (1998) 210–229.
- [33] V. Saxena, S.B. Pope, *Combust. Flame* 117 (1999) 340–350.
- [34] P. Koutmos, *Acta Astronaut.* 46 (2000) 47–53.
- [35] R. Cao, H. Wang, S.B. Pope, *Proc. Combust. Inst.* 31 (2007) 1543–1550.
- [36] K. Gkagkas, R.P. Lindstedt, *Proc. Combust. Inst.* 31 (2007) 1559–1566.